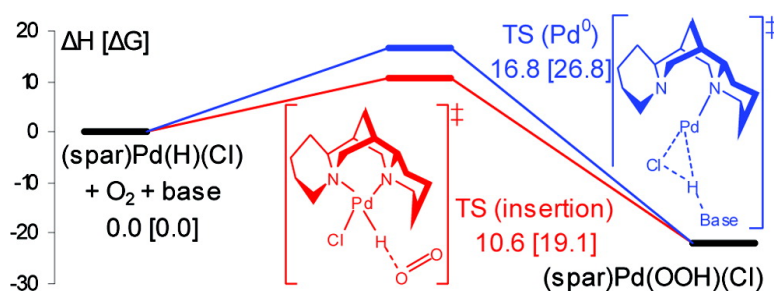Article

Pd-Mediated Activation of Molecular Oxygen: Pd(0) versus Direct Insertion

Jason M. Keith, William A. Goddard, and Jonas Oxgaard

More About This Article

Additional resources and features associated with this article are available within the HTML version:

- Supporting Information
- Links to the 7 articles that cite this article, as of the time of this article download
- Access to high resolution figures
- Links to articles and content related to this article
- Copyright permission to reproduce figures and/or text from this article

View the Full Text HTML

J|A|C|S

A R T I C L E S

Pd-Mediated Activation of Molecular Oxygen: Pd(0) versus Direct Insertion

Jason M. Keith, William A. Goddard, III,* and Jonas Oxgaard*

Contribution from the Materials Process and Simulation Center, MC (139-74), California Institute of Technology, Pasadena, California 91125

Received January 22, 2007; E-mail: wag@wag.caltech.edu; oxgaard@wag.caltech.edu

Abstract: In developing environmentally benign chemistries, it is most important to use dioxygen directly in lieu of toxic and/or corrosive stoichiometric oxidants. Unfortunately, for many processes such direct oxidations have not yet become practical. To help develop such processes, we elucidate here the mechanism for the reaction of molecular oxygen with toluene-solvated palladium−hydride complex using quantum mechanics (B3LYP/LACVP** with the PBF polarizable continuum solvent model) for Pd^{II}−((−)sparteine)-(H)(Cl) in the presence of base, specifically focusing on the pathways proceeding through Pd^0. The lowest barrier Pd^0 pathway proceeds through a rate-determining base-assisted deprotonation of the palladium, followed by the association of molecular oxygen and the subsequent loss of chloride, forming the corresponding η^2-peroxo−palladium complex. We also examine the spin transition and the completion of the reaction to form $PdCl_2$ and H_2O_2. Together with our previously published Pd−H/O_2 direct insertion mechanism, these reports provide a complete mapping of the possible pathways for reoxidation of palladium hydride with molecular oxygen. For this particular system, we conclude that direct insertion is preferred ($\Delta\Delta H^{\ddagger} = 6.2$ kcal/mol, $\Delta\Delta G^{\ddagger} = 7.5$ kcal/mol) and trace this preference to the bidentate character of sparteine and the lack of π-accepting ligands. Suggestions are included for how this preference can be switched.

1. Introduction

Palladium catalysis enables a broad spectrum of selective oxidation reactions of organic substrates, frequently employing molecular oxygen as the stoichiometric oxidant.[1] Oxygen is the ideal oxidant for green chemistry, as it is inexpensive, abundant, noncorrosive, and environmentally benign. Thus, enabling the use of molecular oxygen is highly desirable. Indeed, significant effort has been devoted to this goal, and Pd/O_2 systems have been developed for selective oxidation of alcohols,[2] intermolecular oxidative amination of alkenes,[3] oxidative C−C bond cleavage in tertiary alcohols,[4] intermolecular heterocyclization of alkenes,[5] and the synthesis of hydrogen peroxide.[6] Nevertheless, the subset of oxygen-utilizing Pd systems constitute only a fraction of the important reactions involving Pd systems, leaving a vast pool of potential reactions where use of oxygen as the oxidant would be most valuable.[1]

The palladium-catalyzed oxidations mentioned above are believed to proceed through an "oxidase" pathway, in which oxidation of the substrate by the palladium species occurs first, followed by reoxidation of palladium by O_2.[1a,b] However, the details of this reoxidation are not clear, which significantly hampers the rational design of further uses. Consequently, much work has been performed in an effort to ascertain the mechanism or mechanisms involved, including the necessary spin conversion from triplet to singlet.[1,7−13]

(1) (a) Punniyamurthy, T.; Velusamy, S.; Iqbal, J. *Chem. Rev.* **2005**, *105*, 2329. (b) Stahl, S. S. *Angew. Chem., Int. Ed.* **2004**, *43*, 3400. (c) Gligorich, K. M.; Sigman, M. S. *Angew. Chem., Int. Ed.* **2006**, *45*, 6612. (d) Nishimura, T.; Uemura, S. *Synlett* **2004**, *2*, 201. (e) Stoltz, B. M. *Chem. Lett.* **2004**, 362. (f) Sigman, M. S.; Schultz, M. J. *Org. Biomol. Chem.* **2004**, *2*, 2551. (g) Stahl, S. *Science* **2005**, *309*, 1824. (h) Muzart, J. *Chem. Asian J.* **2006**, *1*, 508.
(2) Sigman, M. S.; Jensen, D. R. *Acc. Chem. Res.* **2006**, *39*, 221. (b) Bagdanoff, J. T.; Stoltz, B. M. *Angew. Chem., Int. Ed.* **2004**, *43*, 353. (c) Jensen, D. R.; Schultz, M. J.; Mueller, J. A.; Sigman, M. S. *Angew. Chem. Int. Ed.* **2003**, *42*, 3810. (d) Schultz, M. J.; Park, C. C.; Sigman, M. S. *Chem. Commun.* **2002**, 3034. (e) Bagdanoff, J. T.; Ferreira, E. M.; Stoltz, B. M. *Org. Lett.* **2003**, *5*, 835. (f) Jensen, D. R.; Sigman, M. S. *Org. Lett.* **2003**, *5*, 63. (g) Steinhoff, B. A.; Stahl, S. S. *Org. Lett.* **2002**, *4*, 4179. (h) Ferreira, E. M.; Stoltz, B. M. *J. Am. Chem. Soc.* **2001**, *123*, 7475.
(3) (a) Rogers, M. M.; Wendlandt, J. E.; Guzei, I. A.; Stahl, S. S. *Org. Lett.* **2006**, *8*, 2257. (b) Lee, J. M.; Ahn, D. S.; Jung, D. Y.; Lee, J.; Do, Y.; Kim, S. K.; Chang, S. K. *J. Am. Chem. Soc.* **2006**, *128*, 12954. (c) Streuff, J.; Hovelmann, C. H.; Nieger, M.; Muniz, K. *J. Am. Chem. Soc.* **2005**, *127*, 14586. (d) Brice, J. L.; Harang, J. E.; Timokhin, V. I.; Anastasi, N. R.; Stahl, S. S. *J. Am. Chem. Soc.* **2005**, *127*, 2868. (e) Timokhin, V. I.; Anastasi, N. R.; Stahl, S. S. *J. Am. Chem. Soc.* **2003**, *125*, 12996.
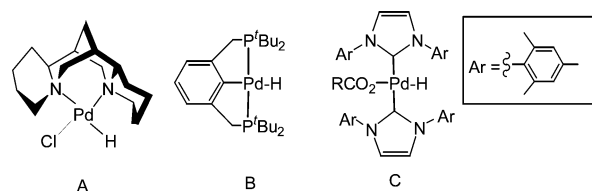
(4) (a) Nishimura, T.; Araki, H.; Maeda, Y.; Uemura, S. *Org. Lett.* **2003**, *5*, 2997. (b) Matsumura, S.; Maeda, Y.; Nishimura, T.; Uemura, S. *J. Am. Chem. Soc.* **2003**, *125*, 8862. (c) Nishimura, T.; Matsumura, S.; Maeda, Y.; Uemura, S. *Tetrahedron Lett.* **2002**, *43*, 3037. (d) Nishimura, T.; Ohe, K.; Uemura, S. *J. Am. Chem. Soc.* **1999**, *121*, 2645.
(5) (a) Piera, J.; Narhi, K.; Backvall, J. E. *Angew. Chem., Int. Ed.* **2006**, *45*, 6914. (b) Trend, R. M.; Ramtohul, Y. K.; Ferreira, E. M.; Stoltz, B. M. *Angew. Chem., Int. Ed.* **2003**, *42*, 2892.
(6) Bianchi, D.; Bortolo, R.; D'Aloisio, R.; Ricci, M. *Angew. Chem., Int. Ed.* **1999**, *38*, 706.
(7) (a) Stahl, S. S.; Thorman, J. L.; Nelson, R. C.; Kozee, M. A. *J. Am. Chem. Soc.* **2001**, *123*, 7188. (b) Konnick, M. M.; Guzei, I. A.; Stahl, S. S. *J. Am. Chem. Soc.* **2004**, *126*, 10212. (c) Clegg, W.; Eastham, G. R.; Elsegood, M. R. J.; Heaton, B. T.; Iggo, J. A.; Tooze, R. P.; Whyman, R.; Zacchini, S. *J. Chem. Soc., Dalton. Trans.* **2002**, 3300.
(8) (a) Landis, C. R.; Morales, C. M.; Stahl, S. S. *J. Am. Chem. Soc.* **2004**, *126*, 16302. (b) Popp, B. V.; Wendlandt, J. E.; Landis, C. R.; Stahl, S. S. *Angew. Chem. Int. Ed.* **2007**, *46*, 601.
(9) Keith, J. M.; Nielsen, R. J.; Oxgaard, J.; Goddard, W. A., III. *J. Am. Chem. Soc.* **2005**, *127*, 13172.
(10) Privalov, T.; Linde, C.; Zetterberg, K.; Moberg, C. *Organometallics* **2005**, *24*, 885.
(11) Denney, M. C.; Smythe, N. A.; Cetto, K. L.; Kemp, R. A.; Goldberg, K. I. *J. Am. Chem. Soc.* **2006**, *128*, 2508.

Scheme 1. Competing Pathways for the Catalytic Cycle of Palladium-Catalyzed Oxidation of Alcohols

Figure 1. Pd species recently examined in the $Pd^0/Pd-H$ insertion debate.
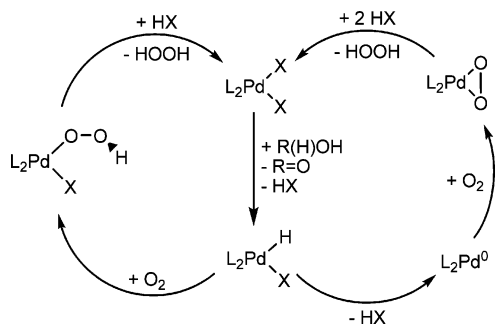
Two competing pathways for the reoxidation step are currently receiving considerable attention in the literature (Scheme 1).[1,7−13] The first involves the formation of Pd^0 through the reductive elimination of HX followed by reaction with O_2 to form an η^2-peroxo species (Scheme 1, right side), whereas the other involves the direct insertion of O_2 into a Pd^{II} hydride (Scheme 1, left side). In particular, several experimental studies on the direct reaction of Pd^0 with O_2 have been reported, demonstrating both the formation of a stable η^2-peroxo Pd^{II} complex (see Scheme 1, right) and the eventual products hydrogen peroxide and $Pd^{II}X_2$, after treatment with HX.[7,8] Although this is not conclusive proof, it demonstrates the feasibility of the Pd^0 pathway under select conditions. In addition to the experimental work, Landis and co-workers used density functional theory (DFT) to examine the feasibility of a spin crossover for several Pd^0 systems and showed that after the triplet Pd^I−superoxide complex is formed, the pathway to the singlet Pd^{II}−peroxo complex is significantly downhill, making the barrier for the spin-crossing practically negligible.[8]

Studies on the direct insertion have been less common. Our group reported DFT studies on a Pd(sparteine) system used in enantioselective oxidation of alcohols, where the direct insertion is calculated to be feasible (Figure 1, species **A**).[9] The insertion mechanism reported therein proceeds through the abstraction of a hydrogen atom by oxygen to form a Pd^I radical T-complex and HOO· which subsequently leads to the formation of triplet palladium hydroperoxo species. After undergoing a spin-flip to form the singlet hydroperoxo species the reaction proceeds through the addition of a proton to form H_2O_2 and the corresponding $PdCl_2$. We concluded that the re-formation of the two radical species and the existence of the cis hydrogen bond acceptor were intimately correlated and removal of the cis hydrogen bond acceptor substantially increased the reaction barrier as the radical pair must first undergo a spin conversion *before* directly forming the singlet hydroperoxo species en route to completing the catalytic cycle. In addition, Privalov et al. conducted investigations on a chelating Pd(phenyl-pyridine)-(H)(pyridine) complex and concluded that direct insertion after O_2 complexation to Pd^{II} was a feasible mechanism for this system.[10]

One of the problems associated with experimental explorations of the direct insertion mechanism is the possibility that a stable palladium hydride could reductively eliminate under reaction conditions preventing the evaluation of the direct insertion method. However, Denney et al. studied a Pd−H complex specifically designed not to allow reductive elimination (Figure 1, species **B**).[11] Upon treatment with O_2, **B** is converted into the corresponding Pd−OOH species and thus experimentally verifies a direct insertion. Subsequently, a report by Konnick et al. appeared where O_2 reacts with the Pd−H complex **C**, forming the corresponding Pd−OOH species. The data presented suggests a reversible reductive elimination pathway, but Konnick et al. could not entirely rule out the possibility of a direct insertion mechanism.[12]

The mechanism of Denney et al.'s (PCP)Pd(H) + O_2 → (PCP)Pd(OOH) reaction was computationally explored by us and was found to react through a mechanism very similar to our previously studied Pd(sparteine) system.[13] However, our results also confirmed that the Pd^0 mechanism is indeed not viable for this system, therefore shedding little light on the competition *between* the two pathways.

Consequently, a study on a system where both pathways are potentially viable would be tremendously useful in understanding what factors enable these mechanisms. Thus, we are now complementing our previous work on the direct insertion with a study of the Pd^0 pathways. In particular, we are focusing on the formation of Pd^0, the subsequent formation of η^2-peroxo Pd^{II}, the spin-crossing from triplet to singlet, and the eventual formation of the corresponding $Pd^{II}X_2$ and H_2O_2 complexes. Herein we will present a detailed mechanistic view of this reaction mechanism. These new results, coupled with our previous work on the direct O_2 insertion mechanism on the identical system, provide a complete picture of both possible pathways and define the preferred path both for our system and those closely related.

2. Computational Methodology

All calculations were performed using the hybrid DFT functional B3LYP, as implemented by the Jaguar 6.5 program package.[14] This DFT functional utilizes the Becke three-parameter functional (B3)[15] combined with the correlation functional of Lee, Yang, and Parr (LYP)[16] and is known to produce good descriptions of reaction profiles for transition metal containing compounds.[17,18] Pd was described with the LACVP** effective core potential and basis set (18 explicit electrons).[19] All other elements were described including the core electrons, using the Pople 6-31G** basis set,[20] but with 3s combination of the six d-like functions reduced to five.

(12) Konnick, M. M.; Gandhi, B. A.; Guzei, I. A.; Stahl, S. S. *Angew. Chem., Int. Ed.* **2006**, *45*, 2904.
(13) Keith, J. M.; Muller, R. P.; Kemp, R. A.; Goldberg, K. I.; Goddard, W. A., III. *Inorg. Chem.* **2006**, *45*, 9631.

(14) *Jaguar 6.5*; Schrodinger, Inc.: Portland, OR, 2003.
(15) Becke, A. D. *J. Chem. Phys.* **1993**, *98*, 5648.
(16) Lee, C.; Yang, W.; Parr, R. G. *Phys. Rev. B* **1988**, *37*, 785.
(17) Baker, J.; Muir, M.; Andzelm, J.; Scheiner, A. In *Chemical Applications of Density-Functional Theory*; Laird, B. B., Ross, R. B., Ziegler, T., Eds.; ACS Symposium Series 629; American Chemical Society: Washington, DC, 1996.
(18) Niu, S.; Hall, B. M. *Chem. Rev.* **2000**, *100*, 353.
(19) (a) Hay, P. J.; Wadt, W. R. *J. Chem. Phys.* **1985**, *82*, 299. (b) Goddard, W. A., III. *Phys. Rev.* **1968**, *174*, 659. (c) Melius, C. F.; Olafson, B. O.; Goddard, W. A., III. *Chem. Phys. Lett.* **1974**, *28*, 457.

All geometries were optimized and evaluated for the correct number of imaginary frequencies through vibrational frequency calculations using the analytic Hessian. Zero imaginary frequencies correspond to a local minimum, whereas one imaginary frequency corresponds to a transition structure.

Implicit solvent effects were calculated with the Poisson−Boltzmann (PBF) continuum approximation,[21] using the parameters $\epsilon = 2.38$ and solvent radius = 2.76 Å. Here we use the solvent accessible surface of the molecular complex built using standard vdW radii. The solvation effects were calculated at geometries optimized for the gas phase.

Using the analytic Hessian we calculated the zero-point energy corrections at 0 K and added this to the solvation correction and the QM energy ($\Delta[E]$) to obtain the enthalpy at 0 K, $\Delta H[0\ K]$. Similarly, the vibrational frequencies were used to calculated the entropy and enthalpy corrections to 298.15 K, to obtain $(\Delta H - T\Delta S) = \Delta G[298.15\ K]$.

On the basis of previous results we expect that relative energies on the $\Delta H[0\ K]$ surface are accurate to ~3 kcal/mol for stable intermediates and to ~5 kcal/mol for transition structures. Probably the relative energies on the $\Delta G[298\ K]$ surface are less accurate, due to the use of the PBF model.[22] This methodology was found to be a an adequate level of theory in our previous study of Pd(sparteine)(Cl)(H) when compared to various other functionals and basis sets.[9]

DFT is formulated in terms of Slater determinants built from Kohn−Sham orbitals that are calculated self-consistently. This process is consistent for states that are well described with closed-shell orbitals (up and down spins in the same orbitals), the normal situation for most DFT applications. However, in the studies carried out here it was necessary to start with a triplet state. With DFT this is done by having two more spin orbitals with up spin than down spin (unrestricted DFT or UDFT). We refer to this as the triplet state, but it need not be an eigenstate of the spin operator, S^2. Rather, it is an eigenfunction of S_z, leading to $M_S = 1$. The problem with this formulation occurs when considering a transition between triplet and singlet states, a topic of this paper. Thus, starting with the true triplet orbitals of O_2 and calculating the energy of the singlet state should lead to a component of $^1\Delta_g$ with an excitation energy of 22.5 kcal/mol. In fact, UDFT gives an excitation energy of 10.5 kcal/mol. The reason is that the $M_s = 0$ wavefunction we consider to describe the singlet state also has a mixture of triplet character. This can be treated by applying the spin projection operator, which will lead to a rigorous energy for the singlet−triplet splitting (20.5 kcal/mol),[23a] but neither the orbitals nor the geometry are optimum after spin projection. Bally and Borden has suggested simply doubling the calculated energy gap in order to approximate the true gap, which in this case yields an energy gap of 21.0 kcal/mol for O_2.[23b] Thus, in the case of O_2 both methods produce similar results. All results reported here are UDFT.

In addition, we used the method of Harvey and co-workers[24] to compute the minimum energy crossing point structure (MECP) between the singlet and triplet potential energy surfaces close to various structures in this study. This technique combines the energies and gradients of the singlet and triplet surfaces into effective gradients that can be followed to locate the position of the MECP structure.

Trimethylamine [N(CH$_3$)$_3$] was used as a model base in place of an additional sparteine molecule, as this considerably cuts down on the computational cost of the calculations. To illustrate the result of this substitution we calculate a ΔH of -0.9 kcal/mol for the reaction

$$\text{sparteine} + [\text{HN(CH}_3)_3]^+[\text{Cl}]^- \rightarrow [\text{H-sparteine}]^+[\text{Cl}]^- + \text{N(CH}_3)_3$$
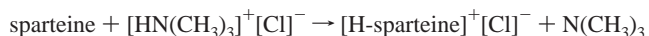
As a result, we expect our use of trimethylamine to impart an artificial increase in barrier heights for the base-assisted reactions, although only at a magnitude of ~1 kcal/mol. Sparteine could potentially present significant steric hindrance to the structures which could increase the energy in those cases. However, several species were examined to a limited extent with a full sparteine base, and we could find no case where the bulk of sparteine seriously impacted any of the pathways presented herein.

It should also be noted that the ligand employed in this study, (−)-sparteine, is one stereocenter removed from C_2 symmetry, and although enantiomerically pure it still presents the dilemma of doubling the number of isomers for most of the steps involved. We found the differences in energy and geometry to be negligible and chose to present only the pathway starting at the (−)-sparteine−Pd^{II}(H)(Cl) species that corresponds with the favorable alcohol oxidation transition state from our previous study on the use of this catalyst in the selective oxidation of alcohols.[25]

In addition, it is relevant to explain that direct formation of Pd^0 during the alcohol oxidation is not feasible in this system. Although one might expect that the (spar)−Pd(Cl)(OC(H)(R)R′) (alkoxide species) could undergo deprotonation by an exogenous base [leading to either [(spar)−Pd^0(Cl)(O=C(R)R′)]$^-$ or directly to (spar)−Pd^0(η^2-O=C(R)R′)] as a corollary to the reactivity of a related N-heterocyclic carbene Pd^{II}(OAc)$_2$-(OH$_2$) complex studied by Nielsen and Goddard,[26] that is not the case here. First, the Pd−H is significantly destabilized in the carbene system as compared to the sparteine system[9,25] and the related pyridine system.[26] Second, formation of HCl or even [base−H]$^+$[Cl]$^-$ in the sparteine system is significantly less favorable than the formation of HOAc in the carbene system. Third, removal of the second proton/H atom from the bound alkoxide (either through deprotonation or β-hydride elimination) is known to be the enantioselective step, and in the case of the possible deprotonation, the activity in the transition state is too far away from the chiral portion of the catalysts to provide the enantioselectivity observed.

3. Results and Discussion

3.1. Base-Assisted Formation of Pd^0. 3.1.1. Primary Pathway. Similar to our previous studies on this system, we chose κ^2-(−)-sparteine−Pd^{II}(H)(Cl) (**1**, Figure 2) as the starting point. Initially an attempt was made to examine the H−Cl reductive elimination pathway leading to a "naked" (−)-sparteine−Pd^0 and HCl, but this was determined to be energetically prohibitive (see section 3.2 for further discussion on this topic). Instead, we elected to focus on a base-assisted deprotonation pathway. Under experimental condition an excess amount of sparteine is present and should, thus, be our first choice of an external base. However, sparteine is also quite large, and to reduce computational time, we elected to model sparteine with the significantly smaller trimethylamine [N(CH$_3$)$_3$]. Introduction of our model base to **1** resulted in the formation of a weakly bound van der Waals complex [κ^2-(spar)Pd^{II}(H)(Cl)]·N(CH$_3$)$_3$ (**2**), with $\Delta H = -0.5$ kcal/mol. The trimethylamine

(20) (a) Hariharan, P. C.; Pople, J. A. *Chem. Phys. Lett.* **1972**, *16*, 217. (b) Francl, M. M.; Pietro, W. J.; Hehre, W. J.; Binkley, J. S.; Gordon, M. S.; DeFrees, D. J.; Pople, J. A. *J. Chem. Phys.* **1982**, *77*, 3654.

(21) (a) Tannor, D. J.; Marten, B.; Murphy, R.; Friesner, R. A.; Sitkoff, D.; Nicholls, A.; Ringnalda, M.; Goddard, W. A., III; Honig, B. *J. Am. Chem. Soc.* **1994**, *116*, 11875. (b) Marten, B.; Kim, K.; Cortis, C.; Friesner, R. A.; Murphy, R. B.; Ringnalda, M. N.; Sitkoff, D.; Honig, B. *J. Phys. Chem.* **1996**, *100*, 11775.

(22) (a) Truong, T. N.; Truong, T. T.; Stefanovich, E. V. *J. Chem. Phys.* **1997**, *107*, 1881. (b) Cramer, C. J.; Thrular, D. G. *Chem. Rev.* **1999**, *99*, 2161. (c) Oxgaard, J.; Muller, R. P.; Periana, R. A.; Goddard, W. A., III. *J. Am. Chem. Soc.* **2004**, *126*, 352.

(23) For further discussion on spin projections of singlet dioxygen see: (a) Xu, X.; Goddard, W. A., III. *Proc. Natl. Acad. Sci. U.S.A.* **1996**, *99*, 15308. For methods on correcting spin contamination in DFT, see: (b) Bally, T.; Borden, W. T. *Rev. Comput. Chem.* **1999**, *13*, 1.

(24) (a) Harvey, J. N.; Aschi, M.; Schwartz, H.; Kock, W. *Theor. Chem. Acc.* **1998**, *99*, 95. (b) Smith, K. M.; Poli, R.; Harvey, J. N. *Chem.—Eur. J.* **2001**, *7*, 1679. (c) Poli, R; Harvey, J. N. *Chem. Soc. Rev.* **2003**, *32*, 1.

(25) Nielsen, R. J.; Keith, J. M.; Stoltz, B. M.; Goddard, W. A., III. *J. Am. Chem. Soc.* **2004**, *126*, 7967.

(26) Nielsen, R. J.; Goddard, W. A., III. *J. Am. Chem. Soc.* **2006**, *128*, 9651.
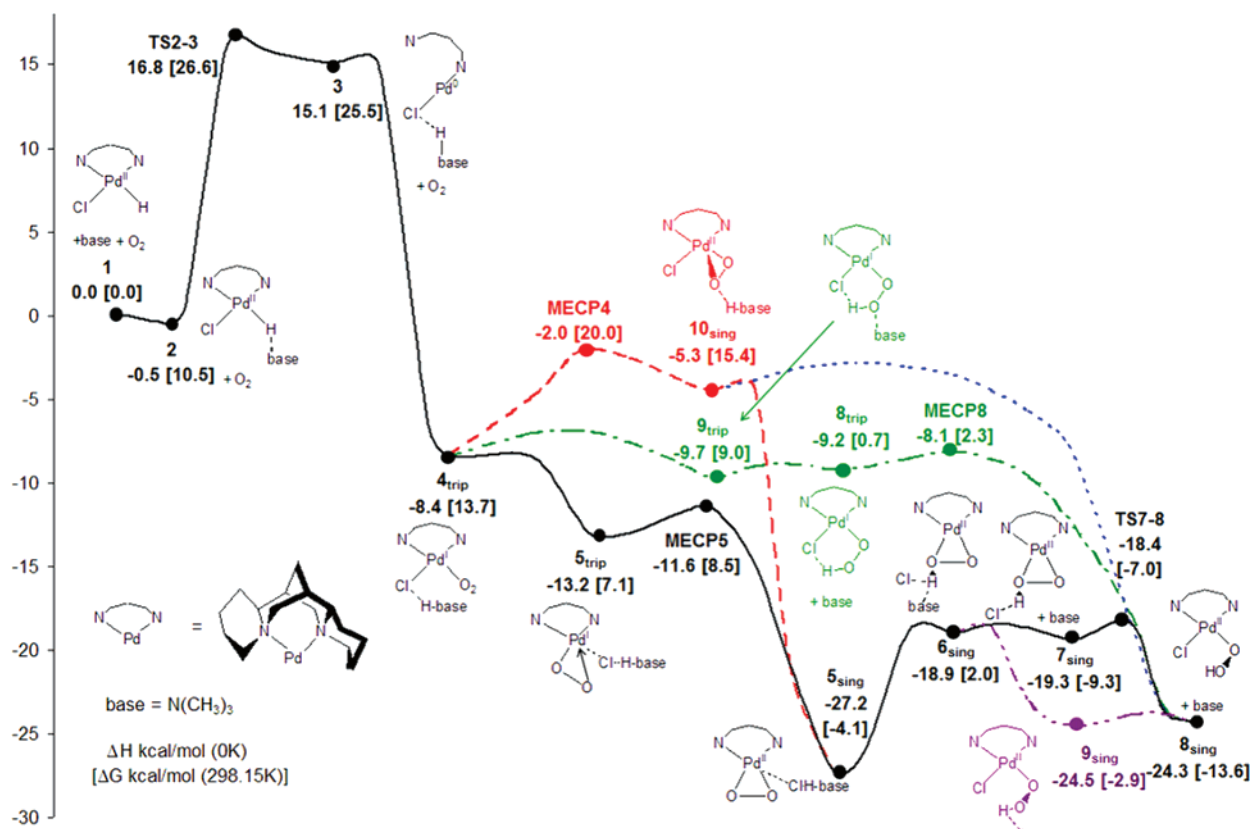
Figure 2. Calculated mechanism for the Pd^0 pathway for $Pd(spar)(H)(Cl) + O_2$ in toluene (base = trimethylamine). Intermediates are shown, while transition states (**TSX−Y**) are shown separately.
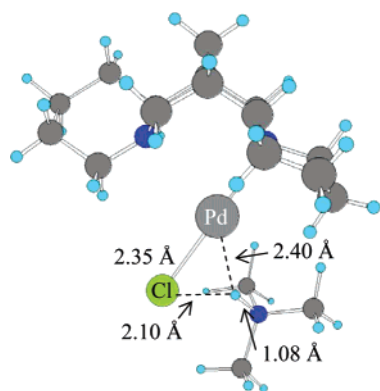

Figure 3. Detail view of **TS2−3**.

remains significantly removed from the Pd species and does not appear to have any significant interaction (N−H distance is >8.0 Å). There is negligible electron transfer between the base and the Pd complex (the Mulliken charges on the trimethylamine and the Pd and adjacent H do not change).

From **2** we found a deprotonation transition state, **TS2−3** (Figure 3), in which the base deprotonates the κ^2-(spar)Pd^{II} complex resulting in the formation of a linear $[\kappa^1$-(spar)Pd^0-(Cl)]$^-$[HN(CH$_3$)$_3$]$^+$ ion pair, **3**. The $\Delta H^{\ddagger}$ for **TS2−3** is 16.8 kcal/mol. **TS2−3** is a fairly late transition state—the Pd−H distance has stretched from 1.52 to 2.40 Å, indicating that the Pd−H bond is completely broken, while the N−H distance has decreased from 8.29 to 1.08 Å, indicating that the N−H bond is fully formed. The imaginary frequency corresponds to a mode in which the proton transfers from the Pd to Cl while keeping the N−H bond intact, indicating the formation of a [(spar)Pd−

Cl]$^-$[HN(CH$_3$)$_3$]$^+$ ion pair. Also of note is that the internal Pd−N$_{spar}$ (cis to Cl) distance has increased from 2.34 to 2.80 Å, indicating a loss of bonding, consistent with the hybridization of the available orbitals on a d^{10} Pd^0 species. As a result of the change in formal oxidation state of the Pd, the Pd−N$_{spar}$ (trans to Cl) and Pd−Cl distances have both increased from 2.18 and 2.35 Å to 2.31 and 2.43 Å, respectively. Finally, the resulting Cl−H distance of 2.10 Å is consistent with that of a hydrogen bond.

From **TS2−3** the energy falls 1.7 kcal/mol when forming species **3**, a linear Pd^0 complex very similar to the preceding transition state. Indeed, the only significant changes are the further stretching of the Pd−H distance (to 2.96 Å), the reduction of the Cl−H distance (to 1.84 Å), and movement of the HN(CH$_3$)$_3$ moiety out of the plane of the molecule spanned by the Pd, the Cl, and both N$_{spar}$'s. Breaking the Pd−Cl bond followed by complete removal of the Cl$^-$[HN(CH$_3$)$_3$]$^+$ ion pair is energetically prohibitive (uphill 13.5 kcal/mol). It could, however, be accessible in related systems and will thus be discussed in detail in section 3.2.

Instead of removing Cl$^-$[HN(CH$_3$)$_3$]$^+$, triplet oxygen was added to **3**. We could not isolate any unbound Pd^0−O$_2$ species, as all attempts immediately optimized to a four-coordinate triplet $[\kappa^2$-(spar)Pd^I(Cl)(O$_2$)]$^-$[HN(CH$_3$)$_3$]$^+$ ion pair, **4$_{trip}$**, with a ΔH of −8.4 kcal/mol. The new Pd−O bond and the electron transfer to form Pd^I are the main factors governing the exothermicity of this step. In this species the two N$_{spar}$'s, the Cl, and the bonding O of the end-on O$_2$ moiety all reside in a square plane. Spin analysis of complex **4$_{trip}$** shows a spin density of 1.16 electrons on the two oxygens (0.62 on the O α to Pd and 0.54

on the O β to Pd), a spin density of 0.67 electrons on the Pd atom, and the remaining spin density (0.17 electrons) distributed over the sparteine and $Cl^-[HN(CH_3)_3]^+$ ion pair, indicating that this complex should be considered a Pd^I species. The O−O bond of 1.32 Å is typical for a peroxyl radical species (1.33 Å in free HO_2), halfway between common single- and double-bond distances of 1.48 and 1.21 Å, respectively. The Pd−N_{spar} distances of 2.39 Å (trans to Cl) and 2.42 Å (cis to Cl) and the Pd−Cl distance of 2.69 Å are elongated compared to those of other Pd^{II} complexes, as expected for a Pd^I center. The new Pd−O and Cl−H bond lengths are 2.17 and 1.93 Å. The energy to break the ion pair at this point is 38.8 kcal/mol on the ΔH surface, and the protonated base will therefore remain associated with the complex until the Pd−Cl bond has been broken.

Species $\mathbf{4_{trip}}$ reacts further through an internal substitution step, in which a Pd−O−O three-membered ring is formed and the Pd−Cl bond is broken. This transition can be described as an intermolecular substitution that involves the simultaneous lengthening of the Pd−Cl bond and the shrinking of the P−O−O bond angle. The energy surface around species $\mathbf{4_{trip}}$ is quite flat, as made apparent by a scan of the Pd−Cl distance. The energy remains almost constant until the Pd−Cl bond is stretched to 3.8 Å ($\Delta E = -10.4$ kcal/mol), at which point the structure relaxes to species $\mathbf{5_{trip}}$. Several transition state calculations were attempted in this area with various starting conditions and geometries, all of which continually tested the surrounding area, maintained sufficiently small gradients, and showed virtually no energy fluctuation, yet all failed to converge to a stationary point. This is most likely a function of the flatness of the surface. Thus, as a result of this exhaustive search and the low energy of the apparent transition point we conclude that there is virtually no barrier for this process.

The new species, $\mathbf{5_{trip}}$, has Pd−O distances of 2.10 and 2.47 Å and an O−O distance of 1.32 Å, forming an unsymmetrical three-membered ring. The Pd−N_{spar} distances are now 2.38 Å (cis to the Pd−O bond) and 2.25 Å (trans to Pd−O bond). The new Pd−Cl distance of 4.30 Å demonstrates that this bond has been completely broken. $[Cl]^-[HN(CH_3)_3]^+$ is, as expected, a bound ion pair (Cl−H distance of 1.84 Å), forming a van der Waals complex with the $Pd(O_2)$ species. The spin densities have changed little from $\mathbf{4_{trip}}$ (0.62 electrons for Pd, 0.60 electrons for O closest to Pd, and 0.66 electrons for O furthest from Pd), implying that this is still a Pd^I species. The calculated ΔH for this complex is -13.2 kcal/mol. The complexation energy of the $[Cl]^-[HN(CH_3)_3]^+$ ion pair is calculated to be 4.4 kcal/mol (see species $\mathbf{12_{trip}}$ in section 3.2.2), thus suggesting that while the ion pair could stay complexed throughout the mechanism, it is not particularly strongly bound. The effect of removing the ion pair is explored in section 3.2.2.

Continuing along the preferred pathway, $\mathbf{5_{trip}}$ now relaxes to $\mathbf{5_{sing}}$ with a ΔH of -27.2 kcal/mol. The MECP for these two surfaces was first explored without the $[Cl]^-[HN(CH_3)_3]^+$ ion pair for computational expedience. (In addition to increasing the computational cost of the optimization, the complexed ion pair also introduces several small oscillating rotational modes that complicate the procedure.) Thus, the corresponding MECP sans ion pair (**MECP12** in section 3.2) was first identified using the methodology by Harvey and co-workers outlined above and has a $\Delta H = -7.9$ kcal/mol. The geometry of the MECP was then frozen and the ion pair reintroduced, followed by an

optimization of the ion pair next to the frozen MECP. This approximate MECP was found to have a ΔH of -11.6 kcal/mol. The geometry of the crossing point is unsymmetrical with respect to the Pd−O−O ring structure, with Pd−O distances of 2.12 and 2.21 Å, the latter being halfway between that of $\mathbf{5_{sing}}$ (2.01 Å) and $\mathbf{5_{trip}}$ (2.47 Å), while the former has remained virtually unchanged from the triplet. Thus, the main nucleic motion associated with the state-crossing is the creation of a Pd−O single bond from the two previously unpaired electrons. Indeed, neither the O−O distance of 1.33 Å nor the Pd−N_{spar} distances of 2.35 (cis to the close O) and 2.29 Å (trans to the close O) have changed noticeably from $\mathbf{5_{trip}}$, which also demonstrates the close proximity of the MECP to the higher energy spin state. This low-energy crossing combined with significant spin−orbit coupling from Pd suggests that the barrier for this formally forbidden spin-flip should be small.

The MECP connects to the stable singlet Pd^{II} species $\mathbf{5_{sing}}$. This complex is structurally similar to $\mathbf{5_{trip}}$, although the Pd−O distances are now almost equivalent (2.01 and 2.02 Å) while the O−O distance is slightly elongated (1.39 Å). The Pd−N_{spar} distances have both decreased to 2.20 Å consistent with the formation of a Pd^{II} species. Indeed, the calculated spin densities (employing an unrestricted wavefunction) on Pd and both O's are now all 0.0, as would be expected from closed-shell Pd^{II} species. The $[Cl]^-[HN(CH_3)_3]^+$ ion pair is still forming a van der Waals complex with the Pd species, with a complexation energy of 8.4 kcal/mol (see species $\mathbf{12_{sing}}$ in section 3.2.2).

Next, the acidic proton from $HN(CH_3)_3^+$ is passed to one of the two O's forming species $\mathbf{6_{sing}}$ with a ΔH of -18.9 kcal/mol. Species $\mathbf{6_{sing}}$ can best be described as a palladium hydroperoxo species with the β-O also acting as a donor ligand, forming an unsymmetrical three-membered ring and with the hydrogen forming a hydrogen bond to the chloride ion. The O−H bond is orthogonal to the square plane, and the O−H−Cl bond angle is 158°. The Pd−O bond distances are 1.98 and 2.17 Å, consistent with one Pd−O covalent bond and one donor−acceptor bond similar to the short bond in species $\mathbf{5_{trip}}$. The O−O bond distance of 1.41 Å is consistent with an O−O single bond. The O−H bond length of 1.04 Å is consistent with a single bond, and the H−Cl distance of 1.90 Å is consistent with a hydrogen bond. The Pd−N_{spar} distances of 2.14 and 2.15 Å are still indicative of Pd^{II} complex. The base is still in the calculation but is merely forming a van der Waals complex with the Pd species. Removal of the base results in species $\mathbf{7_{sing}}$, which is structurally identical to $\mathbf{6_{sing}}$ except for the absence of the base. The complexation energy of the base is very low (0.4 kcal/mol), resulting in a $\Delta H = -19.3$ kcal/mol for $\mathbf{7_{sing}}$.

From $\mathbf{7_{sing}}$, the mechanism proceeds through a substitution where the Cl displaces the weakly bound O (referred to as the β-O above) forming a Pd(OOH)(Cl) species, $\mathbf{8_{sing}}$, through transition state **TS7−8** (Figure 4). The $\Delta H^{\ddagger}$ for **TS7−8** is -18.4 kcal/mol, and it can be described as an associative substitution process in which the Cl approaches from out of the square plane (∼45°) while the Pd−O(β) is dissociating. The Pd−O(β) distance has stretched from 2.17 to 2.28 Å, demonstrating that the Pd−O(β) coordination has not yet completely disappeared, while the Pd−O(α) and O−O distances are unchanged. The Pd−Cl distance has reduced from 3.37 to 3.08 Å but is still significantly longer than the Pd−Cl distance of 2.42 Å in $\mathbf{8_{sing}}$, and the Cl still resides out of the plane. The O−H distance has
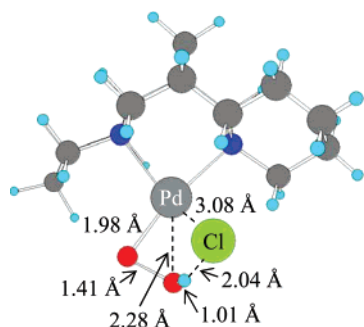
Figure 4. Detail view of **TS7−8**.

decreased from 1.04 to 1.01 Å, while the H−Cl distance has increased from 1.89 to 2.04 Å, both consistent with the weakening of the H-bond. The Pd−N$_{spar}$ distances have remained at ∼2.15 Å.

8$_{sing}$ is a stable Pd^{II} hydroperoxo species with a ΔH of −24.3 kcal/mol. The Pd−O distance of 1.98 Å is consistent with a single bond. The O−O bond distance of 1.43 Å is slightly shorter than the corresponding distance of 1.48 Å in HOOH, while the O−H bond distance of 0.98 Å is almost identical. The Pd−N$_{spar}$ distances of 2.20 (trans to Cl) and 2.24 Å (cis to Cl) and Pd−Cl distance of 2.42 Å are also consistent with Pd^{II} complex. At this point we have merged with the pathway in our previous work on the direct O$_2$ insertion into a Pd−H bond.[9] The remaining steps to form (spar)PdCl$_2$ are described in detail in this previous report and will not be repeated here.

It should also be mentioned that Stahl et al. demonstrated that when CH$_3$CO$_2$H or H$_2$SO$_4$ is added to a bathocuproine−Pd^{II}−η^2-peroxo species it immediately reacts to form H$_2$O$_2$ and the corresponding PdX$_2$ [X$_2$ = (OAc)$_2$, SO$_4$]complex.[7a] This corresponds quite well with our calculated mechanism from **5$_{sing}$** to product.

3.1.2. Alternate Pathways Starting at 6$_{sing}$. We also examined the effect of leaving the base complexed to species **6$_{sing}$** on the further mechanism. The dissociative substitution of the Cl to **6$_{sing}$** results in complex **9$_{sing}$** (structurally identical to **8$_{sing}$**, except for the van der Waals complexed base). ΔH for **9$_{sing}$** is −24.5 kcal/mol, and the complexation energy of the base is thus only 0.2 kcal/mol. Thus, it can be stated that the process from **6$_{sing}$** to **8$_{sing}$** can proceed first by the loss of complexed base followed by substitution of the chloride or vice versa with no relevant energy barriers.

3.1.3. Alternate Pathways Starting at 4$_{trip}$. Although all feasible Pd^0 pathways we found proceed through **TS2−3**, several competitive pathways exist between species **4$_{sing}$** and **8$_{sing}$** (Figure 2, dotted lines). The first obvious choice is to carry out the proton-transfer step immediately. The resulting species, **9$_{trip}$**, is significantly higher in energy than any of the other pathways discussed, although energetically similar to **4$_{trip}$** with ΔH of −9.7 kcal/mol. Upon removal of the base from the system ΔH changes only slightly to −9.2 kcal/mol, and the Pd structure, **8$_{trip}$**, remains the same. At this point we have merged with the direct insertion pathway in our previous paper,[4] and we will not repeat the remaining steps to form (spar)PdCl$_2$ aside from an improved approximation of the barrier for spin crossover **MECP8**, $\Delta H = -8.1$ kcal/mol, as a result of our improved methods concerning MECPs as discussed in section 2. Although this pathway (**4 → 9**) does not seem to have prohibitively high barriers and is competitive with the previous pathway (**4 → 5**),

we believe it is less favorable due to the virtual lack of a barrier from **4$_{trip}$** to **5$_{trip}$** and the observation that the previous pathway remains lower in energy throughout the entirety of the mechanism.

Another alternate direction from species **4$_{trip}$** could be to reverse the ordering of the spin conversion and the intramolecular substitution. It should also be noted that before species **4$_{trip}$** the singlet−triplet splitting is too large to even consider the spin-flip (corresponding to the singlet−triplet separation for free O$_2$, as discussed in our preceding paper).[9] The MECP of these two surfaces (designated **MECP4**) has a ΔH of −2.0 kcal/mol. **MECP4** looks very similar to **4$_{trip}$**, and the only notable geometrical changes include a shortening of the Pd−O distance from 2.17 to 2.01 Å, a lengthening of the Pd−Cl distance from 2.60 to 2.69 Å, and a decrease in the Pd−O−O bond angle from 120.3° to 111.5°.

The hypothetical resulting species **4$_{sing}$** is not stable and immediately relaxes to form species **10$_{sing}$** with a ΔH of −5.3 kcal/mol. **10$_{sing}$** is similar to **4$_{trip}$** except that the O$_2$ species has now formed an unsymmetrical three-membered ring with the Pd perpendicular to the original square plane. The new Pd−O distances are 1.94 and 2.51 Å, while the Pd−Cl distance is 2.61 Å.

From species **10$_{sing}$** there are two pathways resulting in either **5$_{sing}$** or **8$_{sing}$**. In the former, the mechanism would proceed by breaking the Pd−Cl bond followed by relaxation of the Pd−O−O heterocycle. The latter would require the transfer of the proton from the base to one of the two O's, followed by relaxation of the hydroperoxo moiety. However, neither of the two transition states responsible for these mechanisms were explored, as they both occur after **MECP4** which is too high in energy to compete with the pathways which proceed from **4$_{trip}$** to species **5$_{trip}$** and **9$_{trip}$**. That being said, we do expect both transition states to be energetically accessible based on their similarities to the transition between **4$_{trip}$** and **5$_{trip}$** and the transition from **5$_{sing}$** to **6$_{sing}$**, and it is thus not inconceivable that they could be favored in other catalytic systems.

3.2. Unassisted Formation of Pd^0. 3.2.1. "Naked" Pd^0. In the literature, a Pd^0 species that retains the bonding of the two donor ligands (in our case, the κ^2-(−)-sparteine ligand) without any other inner-sphere interactions, or simply "naked", is commonly invoked.[1a,b,7a,b,12] The proposals for this type of mechanism include reductive elimination transition states (which would coincide with the elimination of H−Cl in our system), while some studies have simply examined this type of Pd^0 species as a *possible* intermediate along the catalytic pathway without concern for its origin.[7a,b] For instance, Stahl and co-workers synthesized a bathocuproine−Pd^0 species as well as the corresponding bathocuproine−Pd^{II}−peroxo complex.[7a] Although this bathocuproine system has been shown to be a competent catalyst for the formation of H$_2$O$_2$[27] there is no evidence that the catalytic cycle actually involves this Pd^0 species. Showing that the Pd^0 complex *can* access the catalytic cycle does not prove that Pd^0 *is accessed* during the catalytic cycle, as it is possible that the synthesized Pd^0 complex converts to the active catalyst *prior* to reaction, instead of the other way around. Consequently, in order to ascertain whether the Pd^0 or

(27) Bianchi, D.; Bortolo, R.; D'Aloisio, R.; Ricci, M. *Angew. Chem., Int. Ed.* **1999**, *38*, 706.
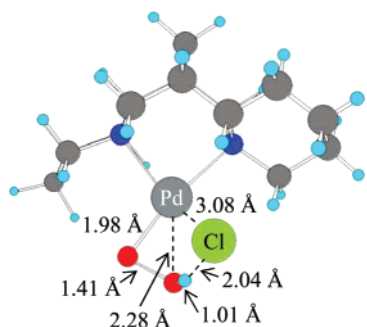
Figure 5. Calculated mechanism for naked Pd^0(spar). Intermediates are shown, while transition states (**TSX−Y**) are shown separately.

the direct insertion pathway is more favorable, an analysis of the entire catalytic cycle must be made.

We find that, for systems with nitrogen ligands where the putative Pd^0 species is prevented from attaining a geometry with the two donor nitrogens at 180° from each other, the energy of the Pd^0 intermediate is prohibitively high. (In contrast, for systems such as Pd(pyridine)$_2$(H)(Cl) the energy of the Pd^0 intermediate is quite accessible, as it is for systems with, for example, a chelating diphosphine ligand.) In our current case, the formation of the naked sparteine−Pd^0 even with the formation of [Cl]$^-$[HN(CH$_3$)$_3$]$^+$ ion pair to help in stabilization is still 28.6 kcal/mol uphill in energy (Figure 5, species **11**), and without the aide of the base it is 51.1 kcal/mol uphill (not shown). Thus, the energy of the intermediate alone is too high to be accessible from species **1**, without considering the energy of the transition states leading to and from **11**. However, although not accessible in this catalytic process, intermediates similar to **11** could very well be accessed in reaction profiles of analogue systems. Moreover, the addition of solvent molecules, molecular oxygen, or other interacting species could realistically lower the energy and play an important role in this and other processes. Indeed, we find that addition of O$_2$ or of a simple model ketone such as acetone can provide a great deal of stabilization to the Pd^0 species, although none of the species we investigated could stabilize **11** enough to make it energetically competitive with the direct insertion pathway. Nevertheless, the results will be discussed in detail and do appear to shed some light on related processes.

3.2.2. Pd^0 with O$_2$. Addition of triplet oxygen to **11** generates **12$_{trip}$**, with an overall $\Delta H = -8.8$ kcal/mol. We could not find a transition state for this process, as **12$_{trip}$** is formed immediately when triplet O$_2$ is introduced to **11**. Indeed, attempts at scanning the energy as a function of Pd−O distance showed a monotonic energy increase with increasing distance, until a plateau was reached.

12$_{trip}$ is an η^2-O$_2$ complex with Pd, which could be characterized as **5$_{trip}$** with the [Cl]$^-$[HN(CH$_3$)$_3$]$^+$ ion pair removed from the system. By adding the [Cl]$^-$[HN(CH$_3$)$_3$]$^+$ ion pair back, this pathway can easily merge to the primary pathway at species **5$_{trip}$** and proceed to products. Alternatively, **12$_{trip}$** could immediately undergo a spin-flip. The MECP for this process, **MECP12**, has an energy of −7.9 kcal/mol and was previously described in detail in section 3.1.1.

The resulting species, **12$_{sing}$**, is identical to **5$_{sing}$** with the [Cl]$^-$[HN(CH$_3$)$_3$]$^+$ ion pair removed from the system, and again this pathway could merge with the primary pathway with the simple addition of the [Cl]$^-$[HN(CH$_3$)$_3$]$^+$ ion pair. The relative ΔH for **12$_{sing}$** is −18.8 kcal/mol.

3.2.3. Pd^0 with Ketone. In addition to adding O$_2$ to **11**, we also considered the possibility that other donating ligands could stabilize the Pd^0 species. As mentioned above, our original focus for the investigation involved the oxidation of alcohols to ketones using a (spar)Pd(Cl)$_2$ catalyst, and as a result there is an abundance of ketone in the reaction mixture. Consequently, we decided to use the ketone acetone as a model donating ligand, designated ket in Figure 5. Addition of acetone to **11** forms the complex **13**, with a $\Delta H = 0.8$ kcal/mol. No transition state was sought for this process as the addition of acetone to species **11** converges monotonically to **13**, much like what was observed for O$_2$. **13** is an η^2-acetone complex with Pd, with a Pd−O distance of 2.07 Å and a Pd−C distance of 2.14 Å. In addition, the C−O distance of 1.30 Å is increased from the free ketone C−O distance of 1.22 Å, while the Pd−C−C bond angles have distorted to 113° and 155°. The Pd−N$_{spar}$ distances of 2.30 (trans to O) and 2.43 Å (cis to O) are both consistent with Pd^0 and similar to what we saw in **5$_{trip}$**.

Although acetone did act to stabilize the Pd^0 species, it does not participate in the remainder of the reaction and will need to be displaced. Despite the fact that this is not the most favorable pathway to proceed from **11** and does not seem to contribute

Figure 6. Detail view of **TS14−15**.

any new information for our specific sparteine system, **13** is similar to known complexes that are known to react to form H_2O_2 and are therefore relevant to the discussion. Of particular note here is the comparison between **13** and the toluene analogue in which toluene is bound to the Pd in an η^2 fashion to the aromatic carbons α and β to the methyl (not shown), $\Delta H = 7.1$ kcal/mol. Since there is no energetic advantage in complexing toluene compared to acetone and both pathways would need to proceed in parallel directions, the toluene-assisted pathway is considered redundant and will not be presented here.

To proceed from **13**, addition of oxygen is required. A weakly bound van der Waals complex, **14$_{trip}$**, is formed when O_2 is added, with a $\Delta H = 0.7$ kcal/mol. The geometry of **14$_{trip}$** has not changed noticeably from **13** despite the addition of O_2, which lies behind the acetone methyls near the Pd square plane. The distances from the Pd to both O's are 5 Å or greater and are indicative of no bonding. Mulliken populations demonstrate that no charge has been transferred between the O_2 and the Pd species, while spin analysis confirms that both unpaired spins still reside on the oxygen.

14$_{trip}$ proceeds through an intermolecular substitution reaction in which the O_2 bonds end on to the Pd, and the Pd−C interaction is broken. The resulting Pd^I species, **15$_{trip}$**, is a square planar Pd complex with both O_2 and acetone bonding with the Pd in an η^1 fashion. The transition state, **TS14−15** (Figure 6), maintains close interaction between the Pd and the O of the acetone while the Pd−C distance has increased resulting in distances of 2.09 and 2.40 Å, respectively. The O_2 is now significantly closer but still unbound with a Pd−O distance of 3.32 Å and an O−O distance of 1.24 Å. The Pd−N$_{spar}$ distances of 2.30 (trans to ket) and 2.49 Å (cis to ket) have not changed significantly from **14$_{trip}$**. $\Delta H^{\ddagger}$ for this step is 4.4 kcal/mol.

The resulting species, **15$_{trip}$**, is significantly more stable, $\Delta H = -8.3$ kcal/mol. The new Pd−O distances are 2.21 (O_2) and 2.23 Å (ket) similar to those seen in previous Pd^I species. The new O−O distance of 1.31 Å is consistent with a peroxyl radical species and further suggests Pd^I species. Indeed, spin analysis shows 0.72 electrons of unpaired spin on the Pd and 1.06 electrons combined on both O's. Of further interest is the C−O distance of 1.26 Å, halfway between that of **14$_{trip}$** and of free acetone, and that the two methyls are still distorted out of plane. The Pd−N$_{spar}$ distances are now 2.32 (trans to ket) and 2.34 Å (cis to ket).

15$_{trip}$ can easily undergo an intramolecular substitution, losing the ketone and forming an η^2-O_2−Pd complex, **16$_{trip}$**, with a $\Delta H = -11.2$ kcal/mol. **16$_{trip}$** can be described as a weakly bound van der Waals complex and is structurally identical to both **5$_{trip}$** and **12$_{trip}$** except for the nonbonded species involved.
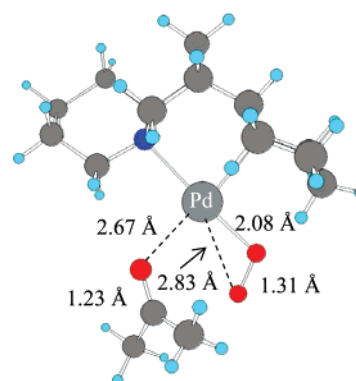
Figure 7. Detail view of **TS15−16**.

TRS15−16 (Figure 7) has Pd−O distances of 2.67 (ket), 2.08 (α-O of O_2), and 2.83 Å (β-O of O_2) demonstrating that the ketone is already unbound, even though the second O has not yet coordinated to the Pd. The O−O distance of 1.31 Å has not changed, but the C−O distance has decreased to 1.23 Å, and the ketone is now planar, just as in free acetone. The Pd−N$_{spar}$ distances are 2.32 Å (formerly cis to ket) and 2.41 Å (formerly trans to ket). Spin analysis show that Pd still has 0.65 electrons of unpaired spin and oxygen has a combined 1.21 electrons of unpaired spin, suggesting that the transition state is still a Pd^I species, whereas **16$_{trip}$** should be considered a Pd^0 species. $\Delta H^{\ddagger}$ for this transition state is −8.1 kcal/mol. At this point **16$_{trip}$** can lose the complexed ketone, resulting in the formation of **12$_{trip}$**, thus merging with the previous pathway and completing the cycle.

4. Conclusion

We conclude that a base-assisted pathway for the formation of Pd^0 from Pd^{II} hydride with the subsequent formation of an η^2-peroxo Pd^0 is energetically accessible for bidentate nitrogen ligand systems such as sparteine. The reaction must proceed as follows:

(1) first through the deprotonation of the hydride to form a linear (κ^1-sparteine)Pd^0−Cl anion (in which one of the two chelating nitrogens has dissociated),

(2) followed by incorporation of molecular oxygen ($O_2{}^t$).

The result is (κ^2-sparteine)Pd^I(Cl)(η^1-O_2), which has one unpaired spin on the Pd and one delocalized over the two oxygens. This rearranges through loss of Cl$^-$ and the associated protonated base coupled with a spin-crossing to the singlet surface. The result is a (κ^2-sparteine)Pd^0(η^2-O_2) singlet. Protonation of this species leads to the formation of a Pd^{II} hydroperoxo complex, and reaction with a second equivalent of HX completes the catalytic cycle by producing Pd^{II}X$_2$ and H_2O_2.

The barrier for the Pd^0 pathway ($\Delta H^{\ddagger} = 16.8$ kcal/mol, $\Delta G^{\ddagger} = 26.6$ kcal/mol, Figure 8) is considerably higher than that of the direct oxygen insertion mechanism previously described for the same system ($\Delta\Delta H^{\ddagger} = 6.2$ kcal/mol, $\Delta\Delta G^{\ddagger} = 7.5$ kcal/mol).[9] We believe these results should apply to all Pd systems which employ bidentate N,N ligands. Indeed, based on these results, we postulate that the bidentate character of the ligand significantly disfavors the palladium(0) pathway, as the resulting d^{10} complex can only be stabilized by one of the two donor atoms. However, this could be alleviated through the use of other donor atoms that are strongly π-accepting, such as P. In addition, disconnecting the tether and allowing the two donor
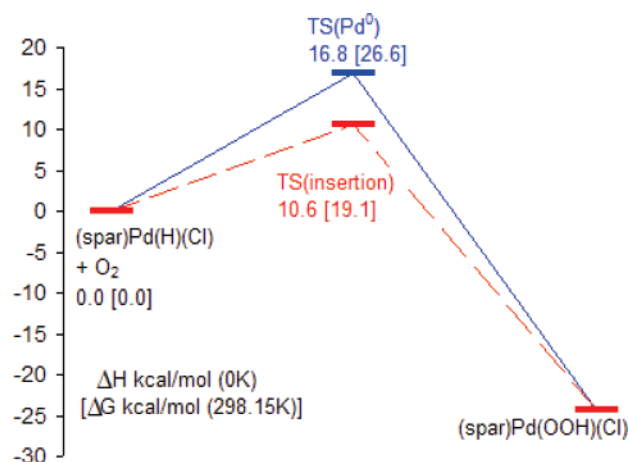
Figure 8. Comparison of Pd^0 (solid line) and insertion (dotted line) energetics for (κ^2-sparteine)Pd(H)(Cl) + O$_2$.

ligands to obtain a trans configuration should also favor the palladium(0) pathway. Finally we speculate that both the insertion and palladium(0) pathways would be stabilized through the employment of more σ-withdrawing ligands, although further testing is required.

Together with our previous report, we now have a complete picture of the two competing pathways at work in a specific palladium oxidase system. We expect this to provide a framework for further studies in this area, and in order to provide further understanding of palladium oxidase chemistry, we are now expanding these studies to such other ligand systems as bipyridine ligands, phosphorus-containing ligands, and tridentate (pincer-type) ligands,

Supporting Information Available: Tables of geometries, ZPE and solvent corrections, and absolute energies of intermediates, as well as geometries, ZPE and solvent corrections, absolute energies, and imaginary frequencies of transition states. This material is available free of charge via the Internet at http://pubs.acs.org.

JA070462D